Morphology Evolution of Miscible Blends Between Crystalline PA6 and Amorphous PA6IcoT

Kun Cao,[1,2] Yan Li,[2] Zhen Yao,[2] Guang-da Zhou,[2] Changchun Zeng,[3,4] Zhi-ming Huang[2]

[1]*State Key Laboratory of Chemical Engineering, Zhejiang University, Hangzhou 310017, People's Republic of China*
[2]*Institute of Polymerization and Polymer Engineering, Department of Chemical and Biological Engineering, Zhejiang University, Hangzhou 310017, People's Republic of China*
[3]*High Performance Materials Institute, Florida State University, Tallahassee, Florida 32310*
[4]*Department of Industrial & Manufacturing Engineering, College of Engineering, Florida A&M University - Florida State University, Tallahassee, Florida 32310*

Received 10 April 2011; accepted 22 June 2011
DOI 10.1002/app.35152
Published online 18 October 2011 in Wiley Online Library (wileyonlinelibrary.com).

ABSTRACT: The morphology evolution of miscible blends of a semicrystalline polyamide 6 (PA6) and an amorphous polyamide 6Ico6T (PA6IcoT) was investigated using an internal Brabender mixer at a temperature range 220–260°C. Morphology of the blends was characterized by scanning electron microscopy (SEM) and laser particle analysis. Temperature rising dissolution was used to separate the different phases of the blends and the phase compositions were determined by Fourier transform infrared (FTIR) spectroscopy. The particle size evolution of the dispersed phase (PA6) was calculated and agreed well with experimental observation. It was found that the particle size was quickly reduced to nanometer scale after several minutes of processing. A convection-diffusion model was adopted to study the phase evolution during melt–melt mixing stage and compute the dimension of each phase. The results strongly support the notion of existence of distinct phases during blending, whose development can be well described by the model. The dispersed phase is reduced mainly by stretching of flow, while the broadening of the blending phase can be primarily attributed to molecular diffusion. The study also suggests the possibility to prepare novel polymer blends with nanometer sized domain of high uniformity. © 2011 Wiley Periodicals, Inc. J Appl Polym Sci 124: 1447–1455, 2012

Key words: polyamide 6; polyamide 6Ico6T; miscible blend; morphology; nanoscale

INTRODUCTION

Blending of polymers is an effective way to prepare versatile materials with desired properties. Investigating morphology evolution of polymer blends is of great practical importance, as morphology is one of the key factors determining the properties of the blends.[1] Such investigation reveals vital information to advance fundamental understanding of many important phenomena such as phase separation and phase inversion, which in turn facilitate process and product design and optimization. Majority of the studies on morphology evolution of polymer blends has focused on immiscible systems.[2–7] Miscible systems, while being studied to a much less extent, have unique features that are of both fundamental and technological interests. While mixing of such systems ultimately leads to homogeneous materials; a broader range of morphology can be realized by controlling the blending process. Understanding the morphology evolution in these systems facilitates technology development to achieve phase states that are inaccessible to immiscible blends. Comparing with immiscible systems, dispersion and deformation mechanism of miscible blend is more complex due to the increased intermolecular contacts.[8]

The morphology of the blends is influenced by several physical phenomena occurring in blending. The initial step is melting of polymers, and understanding the melting mechanism is one of the key aspects in developing general knowledge on blend morphology evolution. For immiscible systems, previous research has showed that the morphology may change significantly during the initial few minutes of mixing.[1,9–13] Burch and Scott studied the softening–melting stage of a miscible blend and found that the morphology development in the melting stage was similar to that for immiscible blends.[14] Another important process in blending of a miscible system is flow-induced change of microstructure.[15] Using miscible materials of relatively low viscosity and zero interfacial tension, the morphology evolvement of droplets during dispersion

Correspondence to: Z. Yao (yaozhen@zju.edu.cn) or C. Zeng (zeng@eng.fsu.edu).
Contract grant sponsor: National Natural Science Foundation of China; contract grant numbers: 50390097, 50773069, 50873090.
Contract grant sponsor: Program for Changjiang Scholars and Innovative Research Team in University.

has been investigated.[16–19] These studies showed that the droplets extended indefinitely due to lacking of the restoring capillary forces. Wetzel and Tucker developed a model and predicted the deformation of an ellipsoidal Newtonian droplet suspended in a second Newtonian fluid with different viscosity and zero interfacial tension.[20] The modeling and experimental results agreed well for the case of shear flow.[21] To date experimental and modeling investigation on miscible blends primarily focused on simple model systems with zero interfacial tension in a simple flow field. Few attempts have been made to analyze the entire blending process of a miscible polymer system and study the morphology development and structure evolution.

In this work, morphology evolution of blends of a semicrystalline polyamide 6 (PA6) and an amorphous polyamide 6IcoT (PA6IcoT) was investigated. This system has been shown to be miscible over all range of compositions.[22–25] Both the melting of polymers and the microstructure change via melt–melt mixing were considered to ascertain information on the phase morphology and phase dimensions, which are essential to understand the morphology transformation during mixing of miscible blend.[26]

THEORY

It is well known that two processes are involved in the formation of a miscible blend: melting of polymer pellets, and melt–melt mixing which includes dispersion of melt and molecular diffusion.[14] Some theoretical background related to these processes is described in detail in the following sections.

Melting of polymer pellets

Although melting of polymer pellets is usually rapid (about 1–3 min) under practical conditions, it has great influence on the blend morphology development. To describe the melting rate of polymer pellets in an internal batch mixer, a two-zone model has been developed.[27] In this model, the batch mixer is divided into two zones: a high shear/high temperature zone and a low shear/low temperature zone. Melting is assumed to takes place primarily in the high shear/high temperature zone. Therefore, the melting rate depends on the number of passage pellets have gone through this zone and the amount of time they experience therein. Based on a number of passage distribution function,[28] the volume fraction of unmelted pellets can be calculated as follows:

$$\phi = \sum_{k=0}^{m-1} \frac{\left(\frac{t}{t_c}\right)^k}{k!} e^{\frac{t}{t_c}} \left(1 - k\beta\sqrt{T - T_D}\right)^3 \quad (1)$$

where m is the number of passages required to melt a pellet. k is a integer between 0 and $m - 1$. t_c is the mean residence time ($t_c = 0.7$ min) in the low shear/low temperature zone and t is the mixing time. T is the material temperature. T_D is related to the melting point and β is related to the initial radius of the pellet.[27] The following values were determined and used in the current study: $T_D = 218°C$ and $\beta = 0.14$.

Melt–melt mixing

Two processes occur during this stage: melting dispersion and molecular diffusion. The melt–melt mixture starts as a two-phase system (matrix phase and dispersed phase). As mixing proceeds intermolecular diffusion between the two phases results in the formation and growth of a new phase, e.g., blending phase. Consequently, the melt–melt mixture becomes a three-phase system.

In this work, a convection-diffusion model, illustrated schematically in Figure 1, was used to describe the melt–melt mixing and evolution of the three

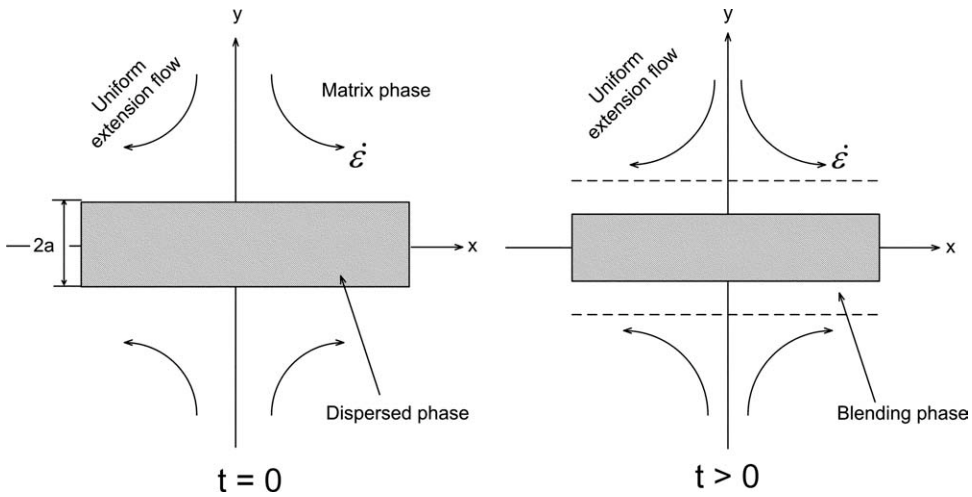

Figure 1 Schematic diagram of phase arrangement and flow field used in the modeling work.

phases. A uniaxial extensional flow was assumed as previous research showed that it was the dominant mechanism for dispersion.[29] The matrix phase (PA6IcoT) was modeled as being continuous with infinite dimensions since in our studies the mass fraction of the dispersed phase (PA6) was low. The dispersed phase was modeled as a thin, striated sheet embedded in the matrix. This is a reasonable initial morphology for the blend because of the lack of interfacial tension between the two phases. For simplification, coalescence effect was not considered. As mixing progresses, the width of the dispersed phase decreases with time via stretching and diffusion, whereas the width of the blending phase increases. Hence, the dimension of each phases were characterized by their width.

Melt dispersion and diffusion were described by the following convection-diffusion equation:[29]

$$\frac{\partial C}{\partial t} - \dot{\varepsilon} y \frac{\partial C}{\partial y} = D \frac{\partial^2 C}{\partial y^2} \tag{2}$$

where C is the dimensionless concentration of PA6, or the mass fraction of PA6 in the dispersed phase; D is the mutual diffusion coefficient, and $\dot{\varepsilon}$ is the extension rate. The initial and boundary conditions are as follows:

$$C_0(y) = C(y,0) = \begin{cases} 1, |y| \le a \\ 0, |y| > a \end{cases} \tag{3}$$

where $2a$ is the initial width of the dispersed phase. The concentration profile can be obtained from eqs. (2) and (3)[29]:

$$C(y,t) = \frac{1}{2} erf \left[\frac{a - y e^{\dot{\varepsilon} t}}{\left(\frac{2D}{\dot{\varepsilon}} (e^{2\dot{\varepsilon} t} - 1)\right)^{1/2}} \right] + \frac{1}{2} erf \left[\frac{a + y e^{\dot{\varepsilon} t}}{\left(\frac{2D}{\dot{\varepsilon}} (e^{2\dot{\varepsilon} t} - 1)\right)^{1/2}} \right] \tag{4}$$

To quantify the phase dimensions, the following criteria were adopted to define each phases: the matrix phase was defined as regions in which the concentration of PA6 was <0.1 ($C < 0.1$), whereas the dispersed phase was defined as regions where the PA6 concentration was higher than 0.9 ($C > 0.9$). Regions with PA6 concentration 0.1–0.9($C = 0.1$–0.9) were considered the blending phase.

The diffusion coefficient D assumed a value of 10^{-17} m^2/s for miscible system.[30] The fitted values of $\dot{\varepsilon}$ used in the model was 0.01 s^{-1} at 10 rpm and a was 2.5×10^{-7} m.

Using the models and parameters describe above, some general phenomena in melt–melt mixing stage were predicted and shown in Figure 2. With increasing mixing time, a rapid increase of width ratio was observed. The width ratio was defined as the ratio of the thickness of the blending phase (l_b) over that of the dispersed phase (l_d). Both were calculated by using eq. (4) and applying the criteria defined earlier for each phases ($0.1 < C < 0.9$ for blending phase and $C > 0.9$ for dispersed phase). The observed increase of the width ratio is a direct result of the fast shrinking of the dispersed phase and accompanying simultaneous growth of the blending phase during melt–melt mixing. The increase of the width ratio is more pronounced during later part of mixing. The effect of diffusion is illustrated by considering the characteristic diffusion time $t_D = l_d/D$,[2,31] which shows significant reduction when mixing time increases [the dash line in Fig. (2)]. At later stage of mixing, the diffusion time approaches zero.

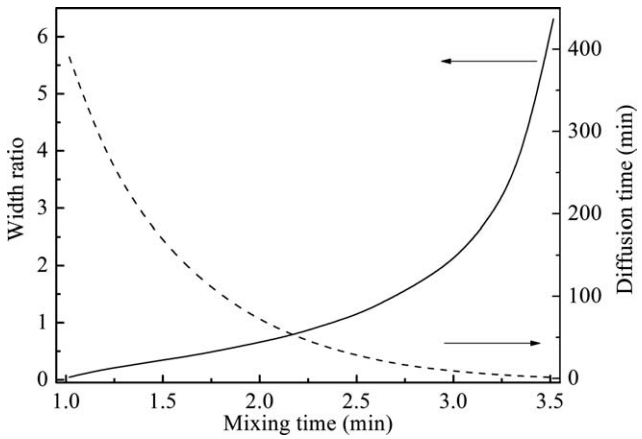

Figure 2 Phase dimension and characteristic diffusion time as functions of mixing time.

From the model prediction, it follows that the melt–melt mixing process can be divided into two stages. In the first stage, flow field induced stretching is the dominant mechanism while molecular diffusion is of lesser importance. This stage is characterized by the significant reduction of the size of the dispersed phase and the concurrent broadening of the blending phase via molecular diffusion. In the second stage in which the diffusion time is very short, mixing is dominated by molecule diffusion. Molecular diffusion eventually leads to the dissolution of the dispersed phase and complete homogenization of the system. The experimental investigation presented below focused on the first stage.

EXPERIMENTAL

Materials

A commercially available PA6 (1030B, UBE Industries, Japan, M_w = 102,000 g/mol) and PA6IcoT (Zytel 330,

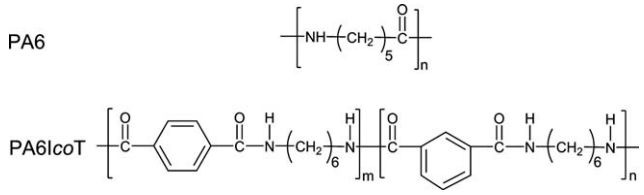

Figure 3 Molecular structures of PA6 and PA6IcoT.

DUPONT, USA, $M_w = 41{,}000$ g/mol) were used to prepare the blends. The chemical structures of polymers are shown in Figure 3. Before use, the materials were dried under vacuum at 80°C for 48 h. Analytical grade dimethyl sulfoxide (DMSO, Hangzhou Changqing Chemical Reagent Co., Ltd, China) was used as the fractionation solvent without further purification.

Blend preparation

The PA6/PA6IcoT blends (10 : 90 wt ratio) were prepared in a Brabender Plasticoder at 220°C and 260°C. The rotation speed of the blades was 10 rpm. Appropriate amount of PA6IcoT pellets were loaded in the Brabender plasticorder and melted first. They system was allowed to reached the designated temperature before PA6 pellets were added. After a predetermined amount of mixing time, the mixer was stopped, and mixtures were immediately taken out and quenched in liquid nitrogen.

Temperature rising dissolution fractionation

The quenched samples were placed in large quantity of DMSO for extended period of time at both 80°C and 100°C, to dissolve the parts of the blends that are soluble at these temperatures. Samples were then filtered under vacuum. Subsequently ample amount of deionized water was added, and the resulting precipitates (filtrates) were also collected by filtration. This procedure was done at both temperatures and both filtrates were collected. In addition, the portion of the sample that was not soluble at 100°C (retentate) was collected as well. All collected samples were dried in vacuum at 80°C for 48 h before further analysis.

PA6IcoT can be easily dissolved in DMSO at 80°C while a higher temperature (110–130°C) is required to dissolve PA6.[32] The temperature rising dissolution fractionation described above therefore may give rise to reasonable separation of the three phases. The portion that was insoluble at 100°C (retentate) may be considered the dispersed phase PA6 (both unmelted and molten part). The fraction dissolved at 80°C is the continuous matrix phase with almost pure PA6IcoT, whereas the part dissolved between 80 and 100°C is predominantly from the blending phase.

Characterization

Fourier transform infrared (FTIR) spectroscopy was employed to determine the compositions of each phase (Nicolet 5700, Thermo). Using a series of PA6/PA6IcoT blends of predetermined compositions, a calibration curve was established by measuring the ratio of the area under 1290 cm^{-1} band versus that under 1545 cm^{-1} band (Fig. 4).

The morphologies of the retentate (fraction that was not soluble in DMSO at 100°C) were observed via scanning electron microscopy (SEM) (Sirion, FEI). The particle size and particle size distribution were characterized by a laser particle size analyzer (Zetasizer3000HSA, Malvern).

The retentate consists of both unmelted and molten portions of the dispersed phase (PA6), and the visual appearance of the two parts is quite different. The unmelted portion appears as dense solid particles while the molten portion appears as loose and flocculent mass. They were easily differentiated by visual observation and manually separated to determine the unmelted fraction of PA6 pellets during melting stage.

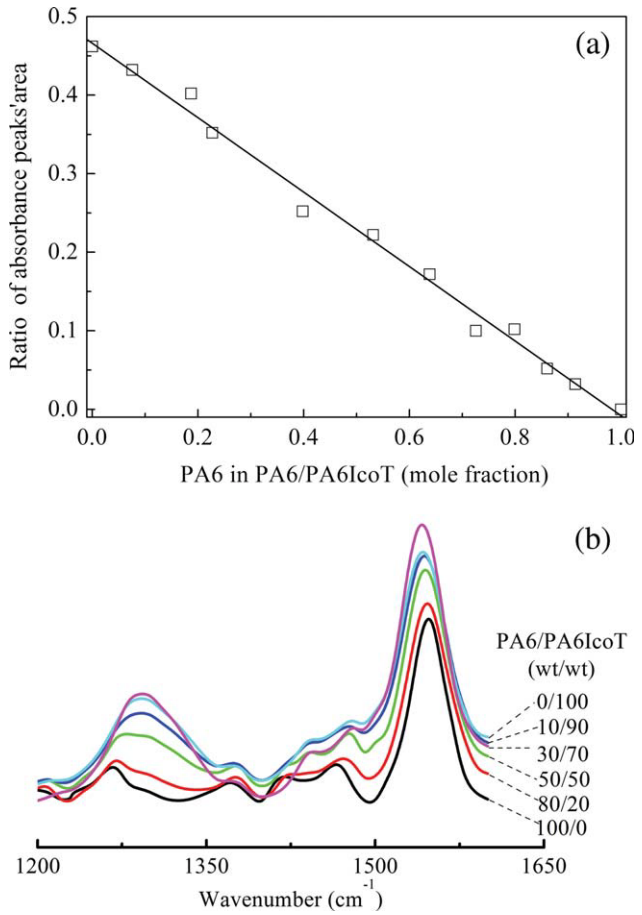

Figure 4 (a) Calibration curve used for determination of the PA6 fraction in blends and (b) FTIR spectra of PA6, PA6IcoT, and PA6/PA6IcoT blends of predetermined compositions. [Color figure can be viewed in the online issue, which is available at wileyonlinelibrary.com.]

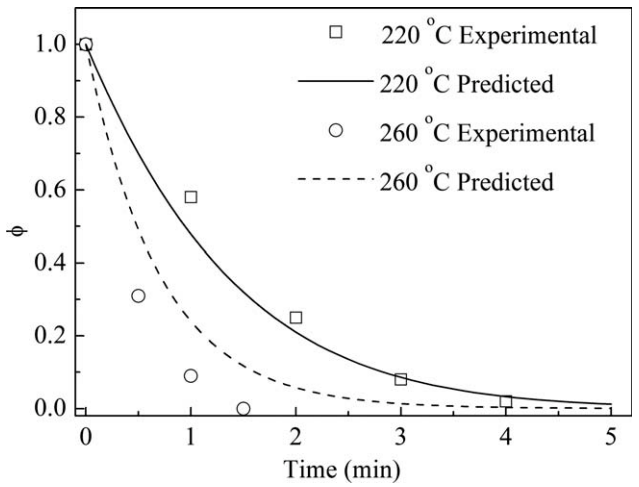

Figure 5 Experimental and predicted values of the unmelted fraction of PA6 pellets in melting of polymer stage.

RESULTS AND DISCUSSION

In this section, we present our experimental investigation on the morphology evolution in blending of PA6 with PA6IcoT and comparison of the experimental results with model prediction. The phase morphology and phase dimensions in melting of polymers and melt–melt mixing stages were both discussed to better understand the morphology development in miscible blend systems.

Melting of polymer pellets

Figure 5 shows the experimental investigation on the melting process and the model prediction at 220 and 260°C. The solid fraction was measured as detailed in the "Experimental" section, whereas theoretical values were computed using eq. (1). The model prediction agrees very well with experimental observations at 220°C and provides reasonable estimation at 260°C. The larger discrepancies between the predictions and experimental observation at 260°C may be partially due to the difficulty to accurately determine the short mixing time. At 260°C, melting proceeds rapidly and was essentially completed after 1 min.

At 220°C, m, the number of passages required to melt a pellet have been estimated to be 5.[27] This value at 260°C is 1 from eq. (5),[33] consistent with the observation of rapid melting at this temperature.

$$\frac{m}{m'} = \frac{\sqrt{T' - T_D}}{\sqrt{T - T_D}} \tag{5}$$

Melt–melt mixing

The SEM images of the dispersed phase (PA6 rich) at different mixing time are shown in Figures 6 (T = 260°C) and 7 (T = 220°C).

As shown in Figure 6(a), the particle size decreased rapidly in the melting stage. The size of the dispersed phase was reduced to <1 μm at the end of the first minute when the melting process was almost completed. Acicular particles were also observed. Figure 6(b) shows the morphology of the dispersed phase after 3 min of mixing. Most particles possessed a polyhedron shape. After 5 min of mixing [Fig. 6(c)], the size of the dispersed particles was reduced to ~ 50 nm. Most particles appeared to be spherical, with remarkable size uniformity. Similar morphology evolution was observed in blends

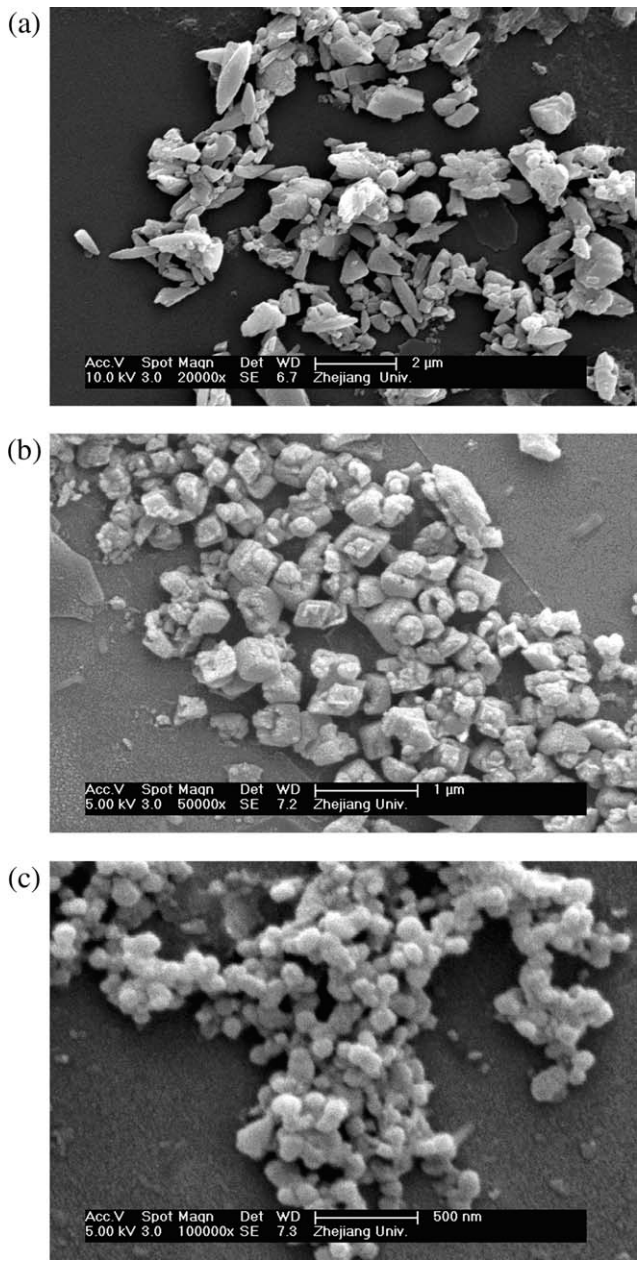

Figure 6 SEM images showing the effect of mixing time on the morphology evolution of the dispersed phase at 260°C: (a) 1 min; (b) 3 min; (c) 5 min.

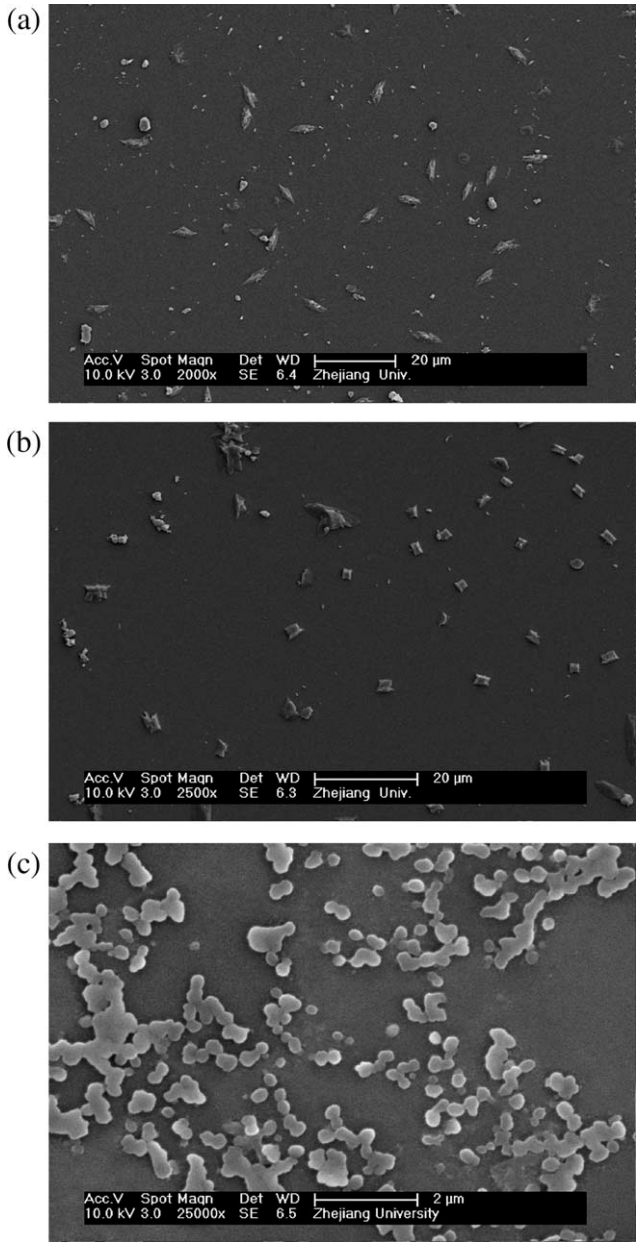

Figure 7 SEM images showing the effect of mixing time on the morphology evolution of the dispersed phase at 220°C: (a) 3 min; (b) 4 min; (c) 8min.

prepared at 220°C (Fig. 7), albeit with a different progression rate and dispersed phase size.

For blends prepared at 260°C, the size distributions of particles obtained from different mixing time were analyzed and shown in Figure 8. The particle size distribution at early mixing stage is rather broad [Fig. 8(a)]. As mixing continues, the particle size decreases and becomes more uniform. After 5 min of mixing, majority of the particles have sizes in the nanometer regime.

As discussed earlier, with the composition and at the mixing temperatures studied herein, the PA6/PA6IcoT blend is a thermodynamically miscible system. A homogeneous system is expected at prolonged mixing time. Nonetheless by controlling the kinetic aspect of mixing, it is feasible to produce blends containing a dispersed phase with tailored domain size and high size uniformity. Formation of such structure is facilitated by the lack of interfacial

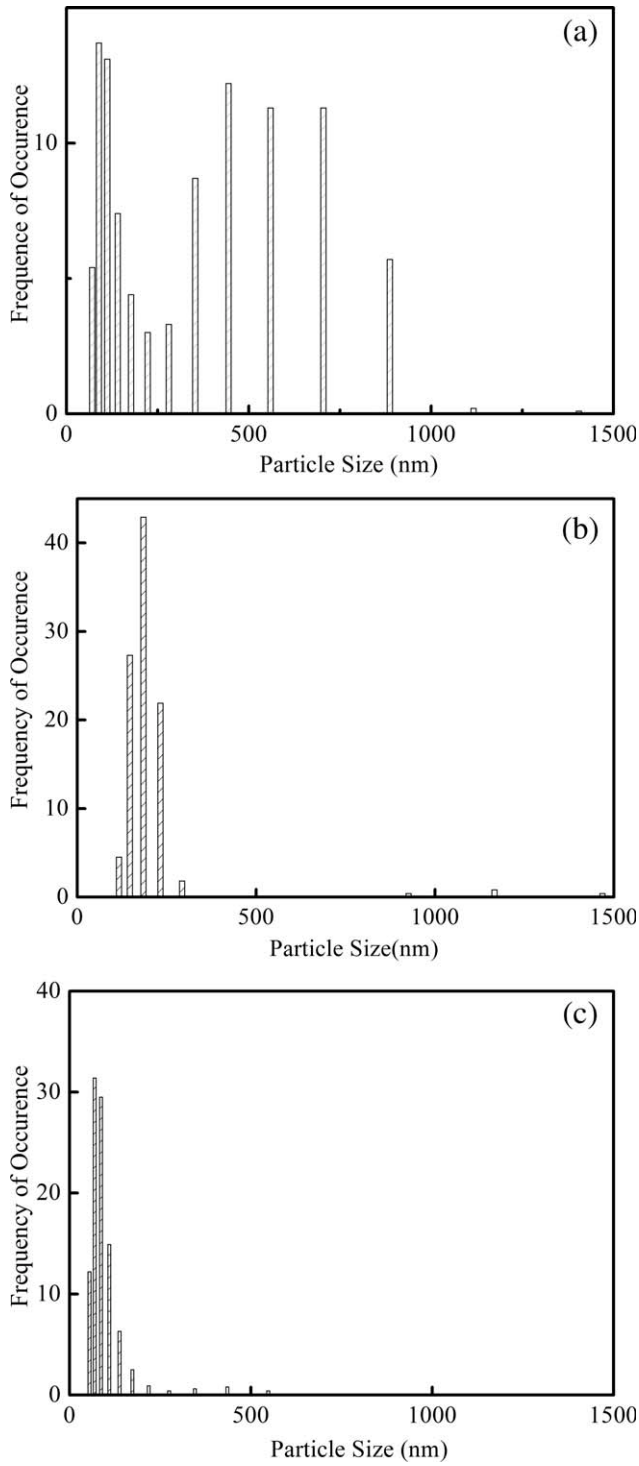

Figure 8 Particle size distribution of the dispersed phase with different mixing times at 260°C: (a) 1 min; (b) 3 min; (c) 5 min.

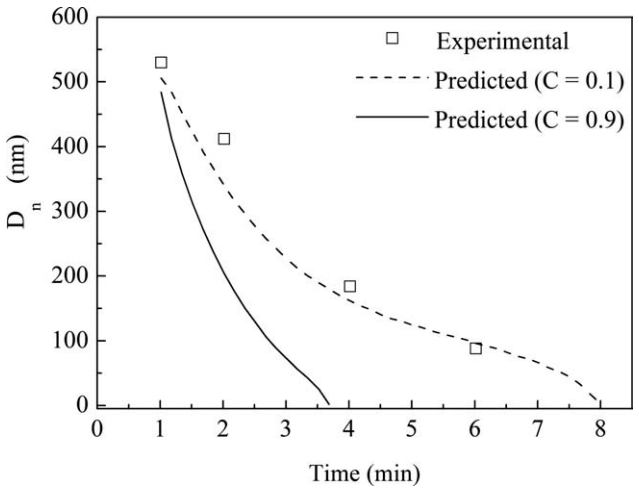

Figure 9 Experimental measurement and model prediction of the particle size of the dispersed phase as a function of mixing time for blends prepared at 260°C.

tension and decreased influence of coalescence in miscible system. As demonstrated in our study, by appropriate combination of mixing temperature and time, the size of the dispersed phase can be controlled within nanometer scale with remarkably narrow distribution. It could be envisioned that if a temperature window exists within which the matrix phase is at the molten state while the dispersed phase is at solid state, additional compounding may be conducted under suitable temperature to further enhance the particle dispersion in the matrix without significantly altering the particle morphology. This will lead to novel polymer blends with well controlled domain size at nanometer scale.

To further understand the morphology evolution, the measured particle sizes were compared with the calculations from the melt–melt mixing model and the results are shown in Figure 9. Recall that the size of the dispersed phase was determined by calculating the concentration profile of PA6 using eq. (4) and applying the criterion that at the boundary the concentration $C = 0.9$. The predicted particle size reduction is much more rapid than the experimental observation. The discrepancy between model prediction and experimental results can be reduced by decreasing the value of PA6 concentration that defines the phase boundary. Rather good agreement was achieved when $C = 0.1$ was applied. Considering that $C = 0.1$ defines the boundary between the continuous phase and the other two phases (dispersed and blending phases), the unexpected agreement suggests that particles recovered from temperature rising fractionation may be a mixture of the dispersed and blending phases. This is addressed in more detail in the following section.

Determination of phases composition

Figure 10 shows the compositions and mass fractions of each phases from the blends with different mixing time, which were obtained by temperature rising dissolution fractionation. Recall that the filtrates from 80°C (Filtrates I) were assigned to be the continuous matrix phase, filtrates from 80 to 100°C (Filtrates II) were from the transitional blending phase; while the insoluble parts at 100°C (retentates) were the dispersed phase. The results suggest, however, that the technique yielded less than satisfactory separation. As shown in Figure 10(a), both filtrates from blends of 1 min mixing time have similar compositions. Moreover, the low concentrations of PA6 in these filtrates suggest that both were from the matrix phases. This argument is further supported by the fact that the two filtrates account for $\sim$ 90% of the total mass, the initial weight fraction of matrix phase PA6IcoT; while the retentate account for $\sim$ 10% of the total mass, the initial weight fraction of the dispersed phase (PA6). The lower than expected concentration of PA6 (0.82 instead of 1) may result from the variation in quantitative determination of concentration by FTIR. Nevertheless, the fractionation analysis strongly suggests that the blend from 1 min mixing time at 260°C is a two-phase system and the blending phase is not present. This observation is also consistent with previous findings shown in Figure 5. After 1 min at 260°C melting of the dispersed phase is near completion, but the blending phase is very small and its development is only at nascent stage.

The filtrates from the blends after 3 and 5 min of mixing [Fig. 10(b) and (c)] were also from the matrix phase, evidenced by the low concentration of PA6 in both. The mass fraction of the retentate is higher for blends with longer mixing time. For example, the blend after 3 min mixing has a retentate mass fraction of $\sim$ 25%, more than twice the initial mass fraction of the dispersed phase. Therefore it is plausible that the retentate contains significant amount of materials from the blending phase. Indeed, the dispersed phase (PA6) concentration in the retentate is only 0.45 rather than close to 1. The mass fraction of the retentate further increases to $\sim$ 30% for the blend with 5 min mixing time, and the concentration of PA6 in the retentate further decrease to 0.35. The fractionation analysis results for blends with different mixing time suggest that as mixing progresses, an increasingly larger amount of materials in the retentate originates from the blending phase.

The above analysis thus suggests that the assumed dispersed phase (the retentate) is in fact a mixture of dispersed and blending phases. Such observation helps elucidate why a better match is obtained between model predicted and experimentally measured particles size when a boundary concentration $C = 0.1$ is applied

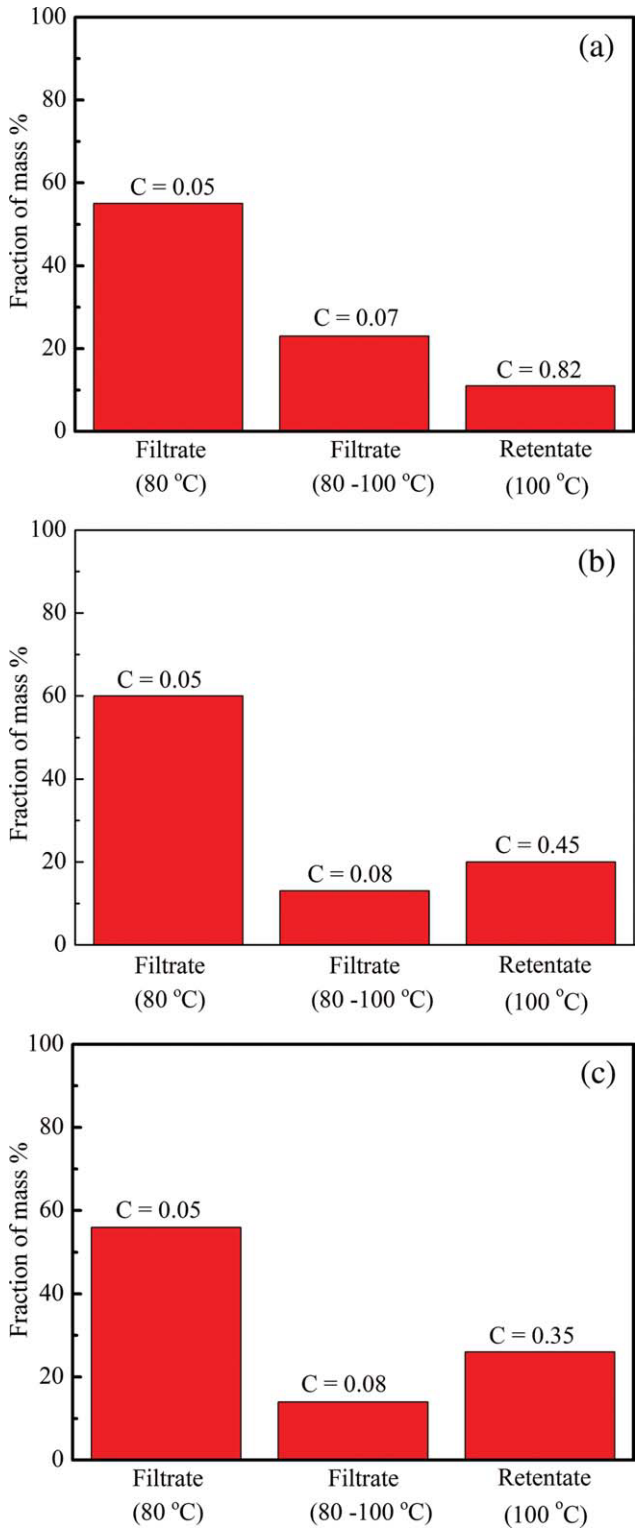

Figure 10 Mass fraction and composition of the fractionated products from blends with different mixing times at 260°C: (a) 1 min; (b) 3 min; (c) 5 min. [Color figure can be viewed in the online issue, which is available at wileyonlinelibrary.com.]

instead of $C = 0.9$ (Fig. 9). The particles observed contain substantial amount of materials from the blend phase and thus have sizes larger than the dispersed phase itself. The boundary condition that defines the phase boundary between the blending and matrix phases is more appropriate for particle size calculation, leading to a better agreement.

The inefficient separation of the blending phase from the other two phases may be attributed to the limited dissolution capability of DMSO at the experimental temperatures and the miscible characteristics of the materials system. Despite the unsatisfactory separation, the results from temperature rising dissolution investigation strongly suggest the existence of distinct stages in the mixing process and evolution of the blending phases.

CONCLUSIONS

Blending of PA6 in PA6IcoT melt occurs in two stages: melting and melting–melting mixing. In the melting stage, the PA6 granules size is rapidly reduced thereby forming a finely dispersed morphology, and the development of miscible blending is similar to that of immiscible blending. During melting–melting mixing, the dispersed phase particles possess various shape and decrease in size. Domains with nanometer size and high uniformity can be obtained by controlling the mixing time and temperature. This may present an innovative approach to prepare new type of nanoscale materials. When the dimension of the dispersed phase reaches nanometer scale, molecular diffusion plays a key role in further size reduction and eventual homogenization.

References

1. Willemse, R. C.; Ramaker, E. J. J.; van Dam, J.; Posthuma de Boer A. Polymer 1999, 40, 6651.
2. Jackson, C. L.; Sung, L.; Han, C. C. Polym Eng Sci 1997, 37, 1449.
3. Wu, S. H. Polym Eng Sci 1987, 27, 335.
4. Sigalov, G. M.; Ibuki, J.; Chiba, T.; Inoue, T. Macromolecules 1997, 30, 7759.
5. Potente, H.; Bastian, M.; Gehring, A.; Stephan, M.; Potschke, P. J Appl Polym Sci 2001, 76, 708.
6. Ziegler, V. E.; Wolf, B. A. Macromolecules 2005, 38, 5826.
7. Liu, H. Z.; Xie, T. X.; Zhang, Y.; Ou, Y. C.; Yang, G. S. J Polym Sci Part B: Polym Phys 2006, 44, 1050.
8. Abtal, E.; Prud'homme, R. E. Polym Eng Sci 1992, 32, 1857.
9. Schreiber, H. P.; Olguin, A. Polym Eng Sci 1983, 23, 129.
10. Plochocki, A. P.; Dagli, S. S.; Andrews, R. D. Polym Eng Sci 1990, 30, 741.
11. Scott, C. E.; Macosko, C. W. Polym Bull 1991, 26, 341.
12. Favis, B. D. J Appl Polym Sci 1990, 39, 285.
13. Scott, C. E.; Macosko, C. W. Polymer 1995, 36, 461.
14. Burch, H. E.; Scott, C. E. Polymer 2001, 42, 7313.
15. Jackson, N. E.; Tucker, C. L., III. J Rheol 2003, 47, 659.
16. Kalb, B.; Cox, R. G.; John Manley, R. St J Colloid Interface Sci 1981, 82, 286.
17. Torza, S.; Cox, R. G.; Mason, S. G. J Colloid Interface Sci 1972, 38, 395.
18. Taylor, G. I. Proc R Soc London, Ser A 1934, 146, 501.

19. Rumscheidt, F. D.; Manson, S. G. J Colloid Sci 1961, 16, 238.
20. Wetzel, E. D.; Tucker, S. L.; Tucker, C. L. J Fluid Mech 2001, 426, 199.
21. Comas-Cardonna, S.; Tucker, C. L., III; J Rheol 2001, 45, 259.
22. Ellis, T. S. Macromolecules 1989, 22, 742.
23. Ellis, T. S. Macromolecules 1991, 24, 3845.
24. Liu, Y.; Donovan, J. A. Polymer 1995, 36, 4797.
25. Siliano, A.; Severgnini, D.; Seves, A.; Pedrelli, T.; Vicini, L. J Appl Polym Sci 1996, 60, 1757.
26. Corte, L.; Leibler, L. Polymer 2005, 46, 6360.
27. Li, H. X.; Hu, G. H. Polym Eng Sci 2001, 41, 763.
28. Tadmor, Z. AICHE J 1988, 34, 1943.
29. Kellogg, L. H.; Turcotte, D. L. Earth Planet Sci Lett 1987, 81, 371.
30. Baird, D. G.; Collias, D. I. Polymer Processing: Principles and Design; Wiley: New York, 1998.
31. Levenspiel, O. Chemical Reaction Engineering, 3rd ed.; Chemical Industry Press: Beijing, 2002.
32. Kartalis, C. N.; Poulakis, J. G.; Tsenoglou, C. J.; Papaspyrides, C. D. J Appl Polym Sci 1924, 2002, 86.
33. Li, H. X.; Hu, G. H. J Polym Sci Part B: Polym Phys 2001, 39, 601.